Transport characteristics of multi-terminal pristine and defective phosphorene systems

Transport characteristics of multi-terminal pristine and defective phosphorene systems

To cite this article before publication: Nayyar Abbas Shah *et al* 2019 *Nanotechnology* in press https://doi.org/10.1088/1361-6528/ab3961

Transport characteristics of multi-terminal pristine and defective phosphorene systems

Nayyar Abbas Shah,[1] L. L. Li,[2,*] Vahid Mosallanejad,[1] F. M. Peeters,[2,†] and Guoping Guo[1,‡]

[1] *CAS Key Laboratory of Quantum Information, and Synergetic Innovation Center of Quantum Information and Quantum Physics, University of Science and Technology of China,Chinese Academy of Sciences, Hefei 230026*

[2] *Department of Physics, University of Antwerp, Groenenborgerlaan 171, 2020 Antwerpen, Belgium*

(Dated: July 8, 2019)

Atomic vacancies and nanopores act as local scattering centers and modify the transport properties of charge carriers in phosphorene nanoribbons (PNRs). We investigate the influence of such atomic defects on the electronic transport of multi-terminal PNR. We use the non-equilibrium Green's function approach within the tight-binding framework to calculate the transmission coefficient and the conductance. Terminals induce band mixing resulting in oscillations in the conductance. In the presence of atomic vacancies and nanopores the conductance between non-axial terminals exhibit constructive scattering, which is in contrast to mono-axial two-terminal systems where the conductance exhibits destructive scattering. This can be understood from the spatial local density of states of the transport modes in the system. Our results provide fundamental insights into the electronic transport in PNR-based multi-terminal systems and into the ability of atomic defects and nanopores through tuning the transport properties.

PACS numbers:

I. INTRODUCTION

Since the discovery of graphene [1], two-dimensional (2D) materials have been in the focus of attention due to their fantastic material properties and promising device application [2, 3]. Recently 2D black phosphorous (BP) has drawn a lot of attention due to its anisotropic electrical and optical properties [4]. Bulk BP is a thermodynamically stable allotrope of elemental phosphorous, which was discovered over a century ago [5, 6]. It is a layered material composed of individual layers that are vertically stacked and coupled via the weak van der Waals (vdW) interaction [7]. Due to the weak vdW interaction, few to monolayer BP (so-called phosphorene) was successfully exfoliated from bulk BP [4, 8]. Phosphorous atoms in monolayer BP are bonded via sp^3 hybridization thereby forming a puckered lattice structure. Phosphorene exhibits the combined properties of a large band gap and a high carrier mobility [8, 9], which makes this 2D material very promising for electronic and optoelectronic applications. A lot of research was carried out to investigate the fabrication, stability, and protection of mono- and/or multi-layer phosphorene at ambient conditions. For instance, a large number of experimental and theoretical studies were carried out to investigate the electro-optical properties of phosphorene and its applications in future electronics and optoelectronics [10–13]. Recently, phosphorene nanostructures such as nanotubes, nanodots and nanoribbons have been investigated for various practical applications [14, 15]. Among them phosphorene nanoribbons (PNRs), a strip of phosphorene, is of particular interest. PNRs have two chiral edge orientations, so-called zigzag and armchair PNR (ZPNR and APNR), which can be fabricated through traditional methods used for graphene nanoribbons (GNRs) [4, 16]. Electronic properties of PNRs are investigated theoretically by using density functional theory (DFT). Nontrivial edge states and a tunable band structure were reported [17–19]. PNR-based structures were also employed to study ballistic transport of charge carriers, Aharonov-Bohm oscillations, and quantum Hall effect [20–22]. It was also shown that the band gap of PNR can significantly be tuned by adatoms, strain and external fields [23–26]. On the other hand, transport study through defective and engineered porous phosphorene was carried out both experimentally and theoretically for mono- and few-atom defects [27–29]. Inherent and engineered defects in nanoribbons change the electronic and transport properties drastically [28, 30]. It was reported that in two-terminal configurations different types of such vacancies alter the band structure differently and modify the conductance of charge carriers [29, 31]. Meanwhile, the transport of charge carriers in quantum devices is extremely sensitive to external connections such as the number and position of terminals to the device [32]. Transport properties of mono-axial two-terminal APNR and ZPNR systems were investigated for both pristine and defective scattering regions [29].

In this paper, we extend the previous two-terminal phosphorene configuration to the multi-terminal case [29]. Meanwhile, the effects of mono to multi-atomic vacancies in the scattering region are investigated. To this end, we consider various device configurations based on multi-terminal PNRs, i.e., L-, T-, and cross-shaped PNRs (LPNR, TPNR, and CPNR), with different types of defects. Conductance and density of states (DOS) show the

*Electronic address: longlong.li@uantwerpen.be
†Electronic address: francois.peeters@uantwerpen.be
‡Electronic address: gpguo@ustc.edu.cn

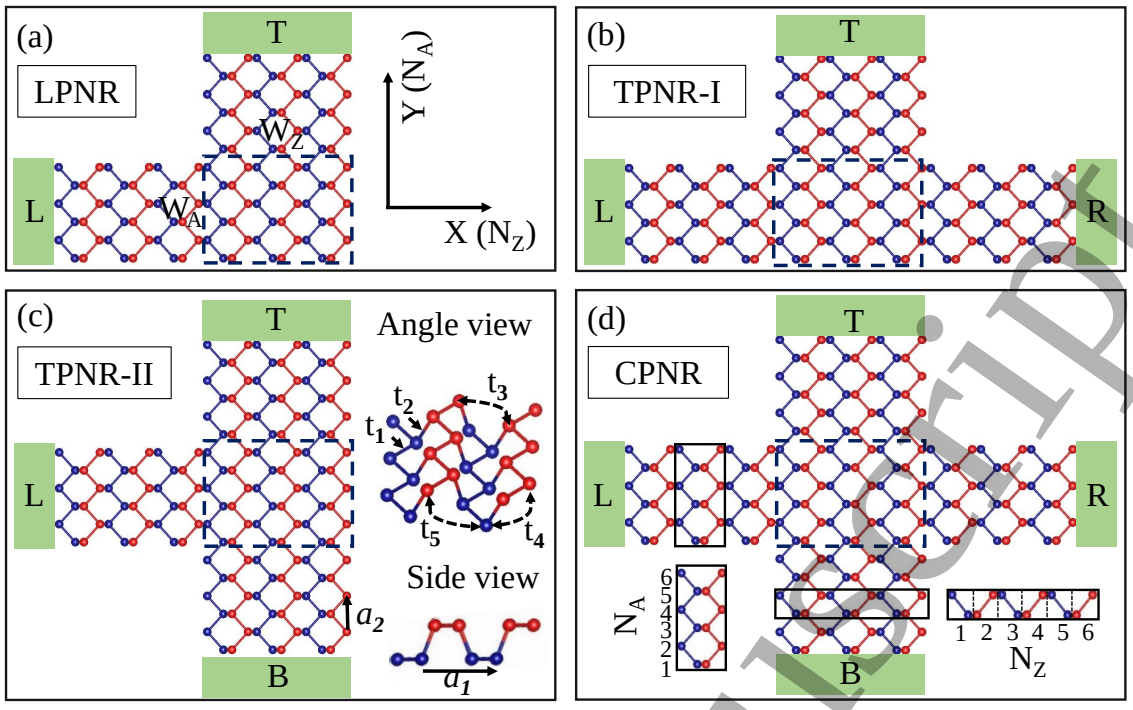

FIG. 1: Schematic diagrams for multi-terminal PNR-based transport systems of various configurations: (a) L-shaped PNR (LPNR) system, (b) and (c) T-shaped PNR (TPNR) systems of type-I and type-II (TPNR-I and TPNR-II), and (d) Cross-shaped PNR (CPNR) system. Here the inset in (c) shows the top and side views of the phosphorene lattice. Where, t_{ij}'s indicate the hopping energies between different atomic sites, L, R, T, and B stand for the left, right, top, and bottom terminals, respectively, and N_A (N_Z) represents the dimer number of armchair (zigzag) terminal.

role of extra-connections. Also, local density of states (LDOS) results are plotted for pristine and defective device structures. Among various widely used computational techniques, we employ the recently proposed multi-terminal recursive Green's function approach with the delicate circular scheme over conventional vertical slicing [33, 34]. Our investigation of the electronic transport in PNR-based multi-terminal systems provides basic insights into their promising applications as building blocks for various quantum devices, such as quantum interference, quantum Hall effect, and electron beam splitting.

This paper is organized as follows. In Sect. (II), we present and explain our device configurations and theoretical formalism. In Sect. (III) and (IV), we discuss the main results of the electronic transport of pristine and defective device systems, respectively. Finally, we conclude our work with a summary in Sect. (V).

II. MODEL AND FORMALISM

To investigate the electronic transport in multi-terminal PNR-based systems, we consider the following device configurations: LPNR, TPNR (both type-I and type-II), and CPNR, as shown in Figs. 1(a)-1(d). Each configuration is composed of two parts, i.e., the finite scattering region and the semi-infinite terminals that are

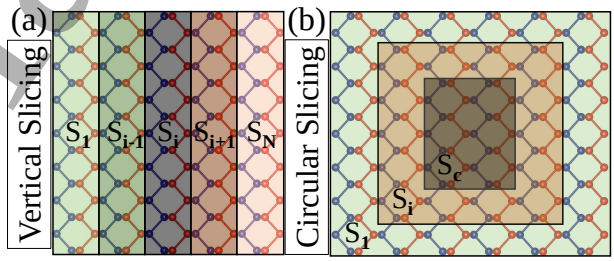

FIG. 2: (a) Vertical and (b) circular slicing schemes of a rectangular scattering region.

labeled by L, R for armchair edges and T, B for zigzag edges. The scattering region has a dimension of $W_Z \times W_A$ in units of nanometers (as distinguished by dotted rectangles). The building blocks (super cells) of the corresponding semi-infinite terminals are marked by solid boxes, as shown in Fig. 1(d). We also depict for an armchair (zigzag) edge termination its corresponding dimer number N_A (N_Z). Furthermore, a top view and a side view of a small piece of PNR is shown in Fig. 1(c) to better visualize the puckered structure of phosphorene, where the lattice constants a_1 and a_2 are equal to 4.57 Å. and 3.34 Å, respectively [19].

We employ the Green's function approach within the tight-binding framework to investigate the electronic and

transport properties of the above-mentioned device configurations. The tight-binding Hamiltonian for phosphorene is given by

$$H = \sum_i \varepsilon_i c_i^\dagger c_i + \sum_{i \neq j} t_{ij} c_i^\dagger c_j, \quad (1)$$

where ε_i, indicates on-site energies in the first term and $c_i^\dagger(c_i)$ is the creation (annihilation) operator. The hopping energies between the neighboring atoms of phosphorene, at sites i and j, are denoted by t_{ij}, as depicted in the right panel of Fig. 1(b). It was shown [35] that for phosphorene on-site energies can be set to zero and hopping energies (in units of eV) are given by $t_1 = -1.220$, $t_2 = -3.665$, $t_3 = -0.205$, $t_4 = -0.105$ and $t_5 = -0.055$. With these parameters this tight-binding model can well describe the band structure of phosphorene in the low-energy region when compared to that obtained by DFT-GW calculations.

Electronic transport in the above-mentioned device configurations can be calculated by using the Landauer-Büttiker approach [36]. Conductance G from terminal (β) to terminal (α) at zero temperature can be written as $G_{\alpha\beta} = (e^2/h)T_{\alpha\beta}$. Here, the Greek's letters α, β refer to as the external terminals (L, R, T, B), and e and h represent the electron charge and Planck's constant, respectively. $T_{\alpha\beta}$ is called the transmission coefficient and is calculated by [33],

$$T = Tr(\Gamma_\alpha G^r \Gamma_\beta G^a), \quad (2)$$

where Γ_α (Γ_β) is the *broadening matrix* that introduces the coupling of the terminal α (β) to the scattering region. G^r ($G^a = G^{r\dagger}$) represents retarded (advanced) Green's function of the scattering region. Broadening matrices are calculated by

$$\Gamma_\alpha = i[\Sigma_\alpha - (\Sigma_\alpha)^\dagger], \alpha = L, R, T, B, \quad (3)$$

where Σ_α is the so-called self-energy matrix for the corresponding terminal and is obtained from $\Sigma_\alpha = H_{S_o\alpha}^\dagger g_\alpha^r H_{S_o\alpha}$. In this relationship, $H_{S_o\alpha}$ represent the connection Hamiltonian for the adjacent super cell of a given terminal to the outermost slice S_o of the scattering region. This matrix is achieved by scanning all atomic sites of the terminal super cell over the S_o sites through Eq. (1). Furthermore, there are only a relatively small number of hopping energies, which are considered up to the first five nearest-neighbor atoms of phosphorene[35]. Thus, the Green's function of the corresponding terminal is attached to the super cell adjacent to the scattering region, which is usually referred to as the surface Green's function, G_α^r. A highly convergent Sancho-Rubio iterative approach is used to calculate the surface Green's function of the terminals [37]. Before calculating the Green's function of the scattering region, there are two quantities of interest, LDOS and DOS. The LDOS is given by [34]:

$$LDOS(E) = -\frac{1}{\pi} Im(G_{i,i}^r), \quad (4)$$

where i indicates the diagonal elements of the retard Green's function G^r at given energy E. And the DOS can be obtained by summation of the LDOS over all the lattice sites for the given energy.

The Green's function of the scattering region is given by

$$G_E^r = [E^+ I - H - \Sigma_i^r]^{-1}, i = L, R, B, T \quad (5)$$

where $E^+ = E + i0^+$, H represent the Hamiltonian of the scattering region, and Σ for the self-energy of the i^{th} terminal. Generally, the direct inversion in Eq. (5) is computationally expensive for larger-scale systems with multi-terminals. Therefore, a recursive Green's function (RGF) method is employed to calculate this inversion of complex systems with multiple external connections. There are various iterative schemes to yield the retarded Green's function recursively. Herein, we choose the circular slicing over vertical and adoptive schemes because of its simplicity and stability to incorporate multiple external connections [33, 34].

Two rectangular regions are shown in Figs. 2(a) and 2(b) which represent the vertical and circular slicing schemes for the PNR-based scattering region. It is important to note that within the tight-binding model we include up to the fifth hopping parameter [35]. Each slice has minimum widths of N_Z=2 and N_A=2 at corresponding interface. Quantum transport studies through two-terminal system usually consider vertical slicing and calculate G^r recursively for each slice[33]. However, this scheme leads to computationally expensive calculations for multi-terminal systems. Thus, a circular slicing as a generic scheme is suitable for more complex systems. By slicing in circular fashion, we scan the whole scattering region till to the deep center S_c, as shown in Fig. 2(b). It can be seen from the figure that the construction of the center slice may have multiple patterns for different dimensions of the scattering region. To calculate the G^r function for multi-terminal system using the circular slicing scheme, it is straightforward to apply the recursive method to the vertical slicing scheme [33, 34].

III. PERFECT PNR-BASED SYSTEMS

First, we characterize the electronic transport in the LPNR system which has two terminals connected non-axially to the scattering region, as shown in Fig. 1(a). Next, we characterize the electronic transport in the relatively complicated TPNR and CPNR systems as shown in Figs. 1(b)-1(d), respectively. The dimension of the scattering region is varied for each configuration to investigate the size dependence of the electronic transport. Specifically we took the width of zigzag (armchair) terminal W_Z (W_A) as 5, 10, 15 and 20 nm, which correspond to the zigzag (armchair) chain number N_Z (N_A) as 24, 46, 68, and 92 (32, 63, 93, and 124). Further, all connected terminals have uniform widths throughout this paper, which can be used to avoid the extra noise in the

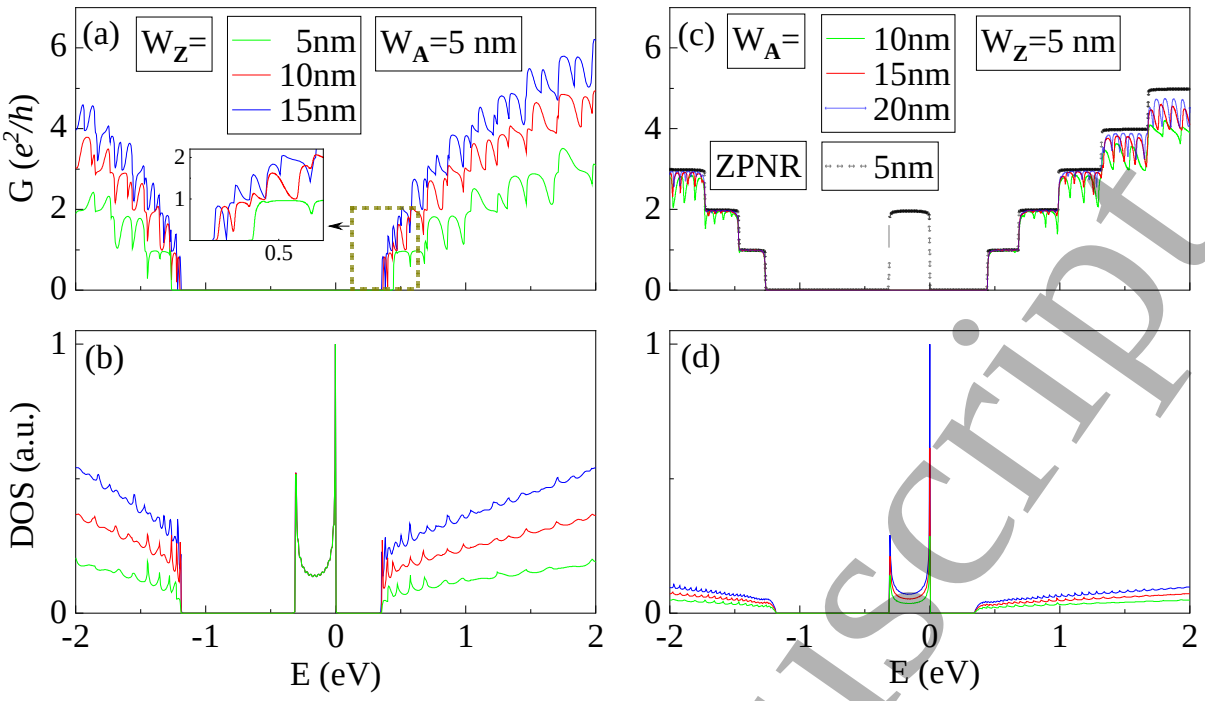

FIG. 3: (a) [(b)] Conductance (DOS) of the LPNR system with constant width of armchair terminal W_A but different widths of zigzag terminal W_Z; and (c) [(d)] conductance (DOS) of the LPNR system with constant W_Z but different W_A. Here, the conductance of mono-axial two-terminal ZPNR system is shown for comparative purposes.

conductance of the transport system due to the interface resistance. [38]

A. Pristine LPNR

In Fig. 3(a), we show the conductance of various LPNR systems with constant width of armchair terminal (W_A=5 nm) but different widths of zigzag terminal ($W_Z = 5, 10, 15$ nm). As can be seen, the conductance increases with the zigzag terminal width. Meanwhile, multiple oscillations are observed in the conductance. The dips in the conductance correspond to anti-resonance states and lead to destruction of quantized plateaus that are the well-known features of mono-axial two-terminal APNR and ZPNR systems. Also, there is a slight reduction in the electronic transport gap by increasing the ratio W_Z/W_A. This behavior is a consequence of the band (mode) mixing between two different terminals and their width-dependent band structure [17]. The gap reduction in the conductance is compensated by increasing the width of zigzag terminal and thus no further reduction would be observed for wider zigzag terminals.

In Fig. 3(c) we show the conductance of the LPNR system with constant width of zigzag terminal (W_Z) but different widths of armchair terminal (W_A). Here the dotted line represents the conductance of the two-terminal ZPNR system (W_Z=5 nm), which is shown for comparative purposes. It is clear that increasing W_A results in less number of anti-resonance dips in the conductance and the conductance restores gradually the quantized plateaus at higher energies which resembles like the two-terminal ZPNR system but with missing in-gap transport modes. The restored quantized plateaus in the conductance are due to the increased number of transport modes in a wider APNR terminal which smears out the conductance oscillations. Moreover, as seen from Figs. 3(a) and 3(c), the conductance of the LPNR system shows a non-metallic behavior. This is because semiconducting modes in the armchair terminal suppress the expected conductance of the ZPNR terminal due to its in-gap modes. This implies that the electronic transport of the LPNR system is predominantly determined by the armchair terminal rather than the zigzag terminal when the Fermi energy of the system is around the electronic transport gap.

B. Pristine TPNR

Next, two types of three-terminal systems, i.e., TPNR-I and TPNR-II systems, as shown in Figs. 1(b) and 1(c), respectively, are investigated and various dimensions are considered for each configuration. In contrast to TPNR-I systems that have two co-axial armchair terminals and one zigzag terminal in the non-axial direction, TPNR-II systems have two coaxial zigzag terminals and one armchair terminal in the non-axial direction.

In Fig. 4(a), we show the conductance for three TPNR-I systems with constant width of armchair terminal (W_A)

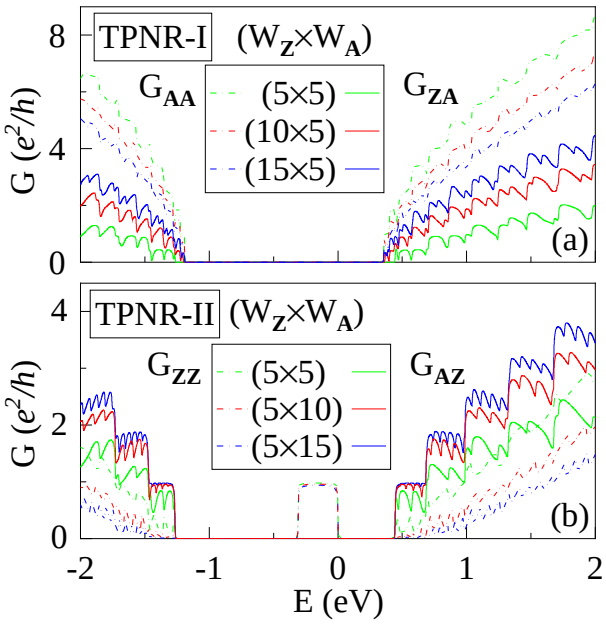

FIG. 4: Longitudinal and transverse conductances of the TPNR-I and TPNR-II systems for different widths of armchair and zigzag terminals (W_A's and W_Z's). Different line colors and styles are used to distinguish the results corresponding to different armchair and zigzag terminal widths.

but different widths of zigzag terminal (W_Z). As can be seen, with increasing W_Z the co-axial (longitudinal) conductance (i.e. G_{AA}) decreases but the non-axial (transverse) counterpart (i.e. G_{ZA}) increases. This is because a wider zigzag terminal contains more transport modes which result in an enhancement in the transverse conductance and a reduction in the longitudinal conductance due to the mode mixing (scattering) with non-axial armchair terminal. We obtain similar results for three TPNR-II systems with constant width of zigzag terminal (W_Z) but different widths of zigzag terminal (W_A), as shown in Fig. 4(b). However, there are still two major differences between TPNR-I and TPNR-II systems: (1) The longitudinal conductance G_{ZZ} of the TPNR-II system has in-gap contribution due to in-gap modes in the zigzag terminal whereas the counterpart G_{AA} of the TPNR-I system does not have due to semiconducting modes in the armchair terminal; (2) The longitudinal conductance G_{AA} is larger than the transverse one G_{ZA} for the TPNR-I system whereas the transverse conductance G_{AZ} is larger than the longitudinal one G_{ZZ} for the TPNR-II system. The second difference is because the electronic transport of the TPNR system is predominantly determined by the armchair terminal, as discussed previously for the LPNR system.

Previously the transport properties of multiterminal graphene nanodevices were investigated using the Landauer-Büttiker approach and the tight binding model [32]. It was shown [32] that the transport properties of graphene-based multi-terminal devices are highly sensitive to the details of the junction region and are drastically different from those on the armchair and zigzag counterparts. Although the conductance of PNR-based multi-terminal systems in this work exhibits some analogous with that of graphene-based multi-terminal systems in that work [32] at high energies, while it differs remarkably at low energies (e.g. around the Fermi energy): In contrast to graphene-based T-shape systems, TPNR-II shows zero transverse conductance for all values of N_A and in-gap conductance plateau between axial zigzag terminals.

C. Pristine CPNR

CPNR is composed of two pairs of semi-infinite armchair and zigzag terminals which are connected to scattering region, as shown in Fig. 1(c). Here we set the CPNR system to fixed dimensions of $W_Z \times W_A = 5 \times 5$ nm and we set the injection source at the armchair or zigzag terminal. In Figs. 5(a) and 5(b), we show the longitudinal and transverse conductances for the armchair and zigzag injection sources respectively, and for comparative purposes we also show the conductances of mono-axial two-terminal APNR and ZPNR systems for the corresponding injection sources. As can be seen, both the longitudinal and transverse conductances (G_{AA}, G_{AZ}, G_{ZA} and G_{ZZ}) of the CPNR system are smaller than the conductances (G_{APNR} and G_{ZPNR}) of the corresponding mono-axial two-terminal systems (APNR and ZPNR), which is irrespective of the injection source. This is due to the presence of the scattering region in the CPNR system, which results in the mode mixing (scattering) between the armchair and zigzag terminals, as discussed previously for the LPNR and TPNR systems. Again, there are no in-gap conductance in the CPNR system because the electronic transport is predominantly determined by the armchair terminal (not the zigzag terminal) which has only semiconducting modes (no in-gap modes).

Moreover, for both the armchair and zigzag injection sources, the transverse conductance G_{AZ} and G_{ZA} have almost the same magnitude. However, the longitudinal conductances G_{AA} and G_{ZZ} differ significantly: G_{ZZ} has a larger deviation from G_{ZPNR} than G_{AA} from G_{APNR}. These features can be understood with the spatial LDOS of the transport modes. In Figs. 5(c)-5(f), we show the spatial LDOS of the transport modes at two given energies, denoted by E_1 and E_2, which are the energies of the third (first) and seventh (third) transport modes of the armchair (zigzag) injection source. As can be seen, for the injection source at the armchair (zigzag) terminal, the high-energy (lower-energy) modes are mixed with the low-energy (high-energy) modes in the zigzag (armchair) terminal. And the transport modes are more significantly scattered for the zigzag injection source than for the armchair injection source. This can explain why G_{ZZ} has a larger deviation from G_{ZPNR} than G_{AA} from G_{APNR}.

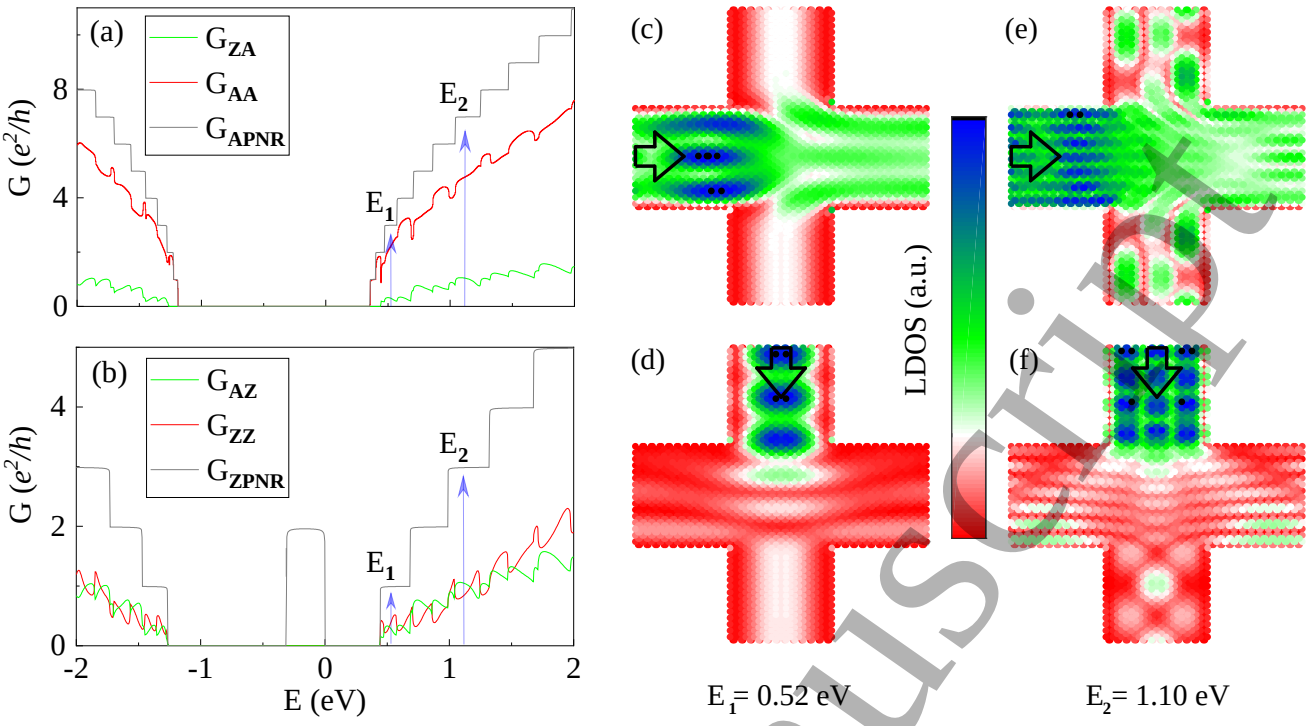

FIG. 5: Quantum transport in the CPNR system with constant widths of armchair and zigzag terminals ($W_A \times W_Z = 5 \times 5$ nm): (a)-(b) Transverse and longitudinal conductances; (c)-(f) Spatial LDOS of the transport modes at two given energies E_1 and E_2 as indicated. Here the injection source is set at the left armchair terminal [(c)-(e)] or the upper zigzag terminal [(d)-(f)].

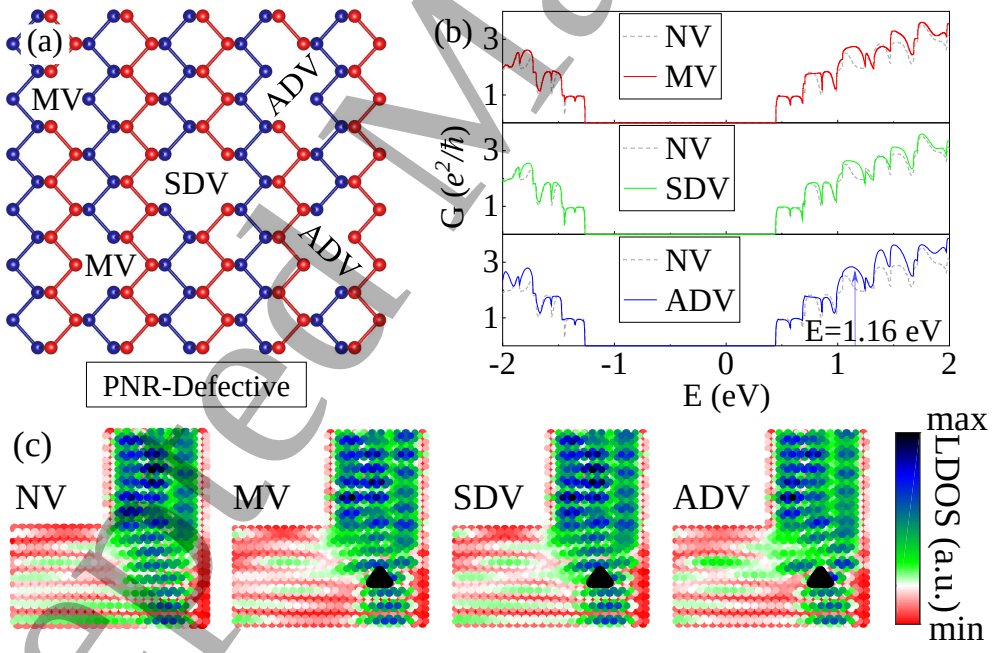

FIG. 6: (a) Three types of intrinsic defects (vacancies) schematically shown with different notations, i.e., MV, SDV, and ADV, as indicated. (b) Conductance of the defective LPNR with MV, SDV and ADV and of the pristine (no-vacancy, NV) system. (c) Spatial LDOS for the cases of NV, MV, SDV, and ADV calculated at $E = 1.6$ eV. Here the solid (dashed) curves represent the results of the defective (pristine) conductance and the black triangle represents the position of atomic vacancy in the LDOS plots.

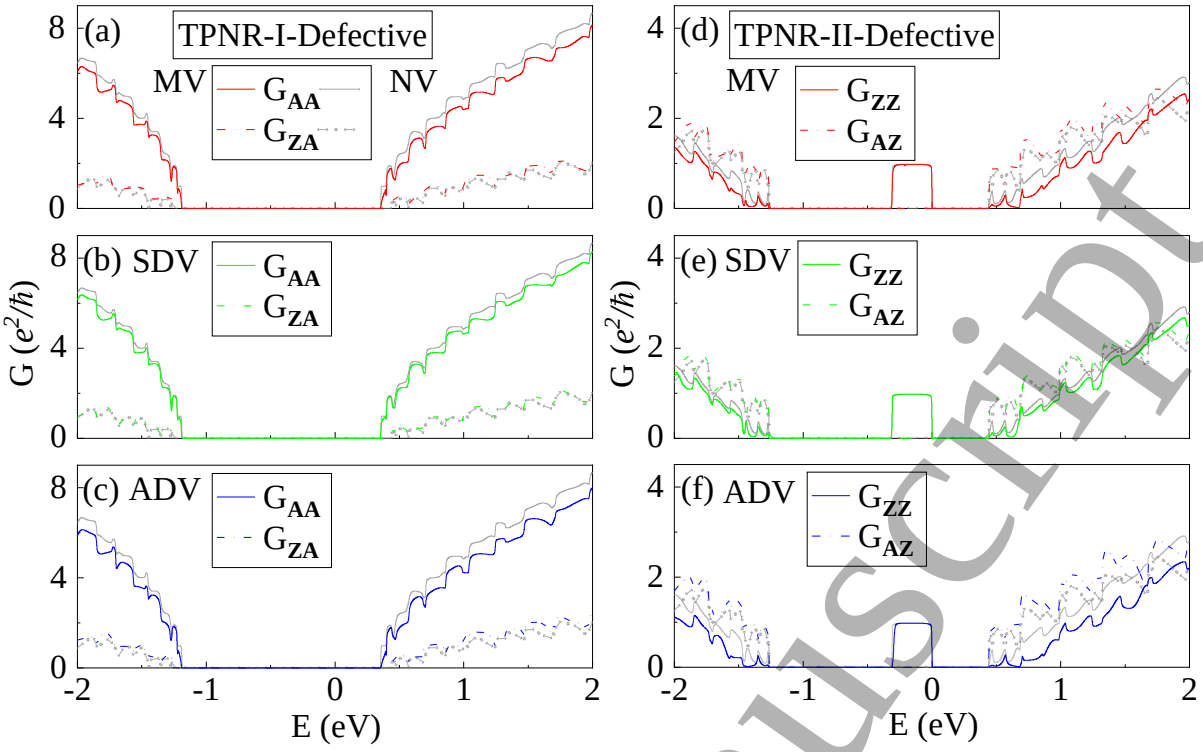

FIG. 7: Conductances of the defective TPNR-I and TPNR-II with MV, SDV, and ADV and of the pristine system: (a)-(c) for TPNR-I and (d)-(f) for TPNR-II. Here the longitudinal (transverse) conductances G_{AA}, G_{ZZ} (G_{ZA}, G_{AZ}) are shown by solid (dashed) curves.

IV. DEFECTIVE PNR-BASED SYSTEMS

In this part, we investigate the electronic transport in defective PNR-based systems for above mentioned configurations, i.e, LPNR, TPNR, and CPNR. We consider two different types of lattice defects, i.e., intrinsic and extrinsic defects. Intrinsic defects refer to vacancies with one or two missing atoms and have two typical types: mono- and di-vacancies (MV and DV). Recently, atomic vacancies were experimentally observed on the surface of black phosphorus [28]. Further, each DV can be categorized into symmetric and asymmetric DV (SDV and ADV) by its nature, where the term "symmetric" ("asymmetric") refer to identical (non-identical) phosphorous atoms in upper and lower atomic sublayers due to missing atoms [39]. Extrinsic defects refer to a bunch of missing atoms, so-called nanopores. Recently it was shown that atomic nanopores can be engineered experimentally in phosophorene systems [27]. We organize this section as follows: First, the influence of intrinsic defects (vacancies) on the electronic transport is examined for the LPNR, TPNR, and CPNR configurations. Later, the effect of extrinsic defects (nanopores) with various shapes are investigated and are compared with intrinsic defects. Further in this section, we consider the scattering region of fixed dimensions, i.e. $W_Z \times W_A = 5 \times 5$ nm, in order to focus on the effect of missing atoms.

A. Defective LPNR

All atomic vacancies (MV, SDV and ADV) are schematically shown in Fig. 6(a). We show in Fig. 6(b) the conductance of the defective LPNR with MV, SDV, and ADV and of the pristine system. As can be seen in Fig. 6(b), these intrinsic defects can give rise to an increase in the conductance between non-axial terminals of the defective LPNR when compared to the pristine system with no vacancy (NV). This increase in the conductance is more profound at the modes with higher energies and the deviation from the pristine system is more significant for the cases of ADV and MV than for the case of SDV. Intuitively, atomic vacancies behave like scattering centers which should lead to a decrease in the conductance. For instance, previously it was shown that atomic vacancies lead to only reduction in the conductance [29] of mono-axial two-terminal PNR-based systems. However, the enhanced conductance of the defective LPNR system, as observed here, shows somehow constructive rather than destructive scattering by atomic vacancies. This implies that atomic vacancies can enhance the electronic transport in non-axial two-terminal PNR-based systems. In order to understand this counter-intuitive feature, we need to look into the spatial LDOS of the defective LPNR with MV, SDV, and ADV and of the pristine system (NV), as shown in Fig. 6(c). It can be seen from Fig. 6(c) that the transport direction of electrons

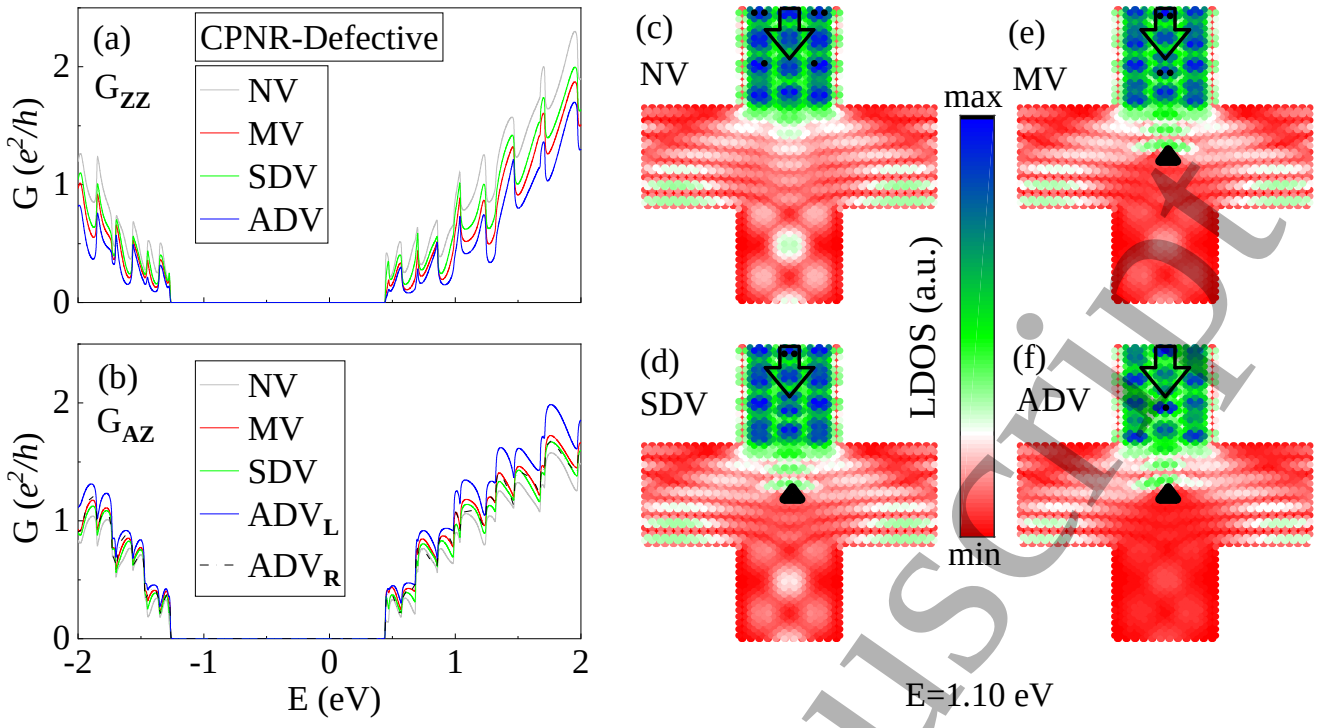

FIG. 8: (a)-(b) Longitudinal and transverse conductances (G_{ZZ} and G_{AZ}) of the defective CPNR with MV, SDV and ADV and of the pristine system (NV); (c)-(f) Spatial LDOS of the transport modes with energy $E = 1.1$ eV for the cases of NV, MV, SDV, and ADV, as indicated. Here, the injection source is set at the upper zigzag terminal and the solid triangles in (e)-(f) indicate the positions of MV, SDV, and ADV in the defective CPNR.

can be scattered orthogonally to their initial direction by atomic vacancies and thereby enhancing the conductance between non-axial two terminals.

B. Defective TPNR

In Figs. 7(a)-7(c), we show the conductance of the defective TPNR-I with MV, SDV, and ADV and of the pristine system (NV). Here the longitudinal (transverse) conductance G_{AA} (G_{ZA}) are shown by solid (dashed) curves. It is observed that the longitudinal (transverse) conductance of the defective system shows a decrease (an increase) when compared to that of the pristine system and this decrease (increase) is more pronounced for higher-energy transport modes. These results are consistent with those previously discussed for defective non-axial LPNR systems and with those obtained for pristine mono-axial PNR systems [29]. And the effect of ADV is more significant than that of SDV and is almost twice as that of MV. In Figs. 7(d)-7(f), we show the longitudinal (transverse) conductance G_{ZZ} (G_{AZ}) of the defective TPNR-II with MV, SDV, or ADV and of the pristine system (NV). It is observed that the in-gap conductance of the defective system is the same as that of the pristine system and remains unchanged for all types of atomic vacancies. This is due to unaffected edge modes localized at one zigzag edge. However, the magnitude of the in-gap conductance of the defective system is reduced by half when compared to that of the ZPNR system due to the missing of the other zigzag edge.

C. Defective CPNR

In this part, we investigate the defective CPNR with intrinsic defects (vacancies) and extrinsic defects (nanopores). For all cases, the injection source is set at one of the two zigzag terminals (e.g. the top one) and furthermore the dimension of the scattering region is set to $W_Z \times W_A = 5 \times 5$ nm.

In Figs. 8(a) and 8(b), we show the longitudinal and transverse conductances (G_{ZZ} and G_{AZ}), respectively, of the defective CPNR with MV, SDV, and ADV and of the pristine system (NV). As can be seen, these intrinsic defects result in a decrease (an increase) in the longitudinal (transverse) conductance G_{ZZ} (G_{AZ}) of the pristine system. It is observed that for G_{ZZ} ADV results in a more significant reduction that SDV and the reduction is almost twice that of MV. Assuming the injection source set at the top zigzag terminal, G_{AZ} exhibits two different results in the case of ADV, as shown in Fig. 8(b) and labeled as ADV_L and ADV_R in the figure, where the former (latter) one is induced by the charge current between the left (right) armchair terminal and the zigzag

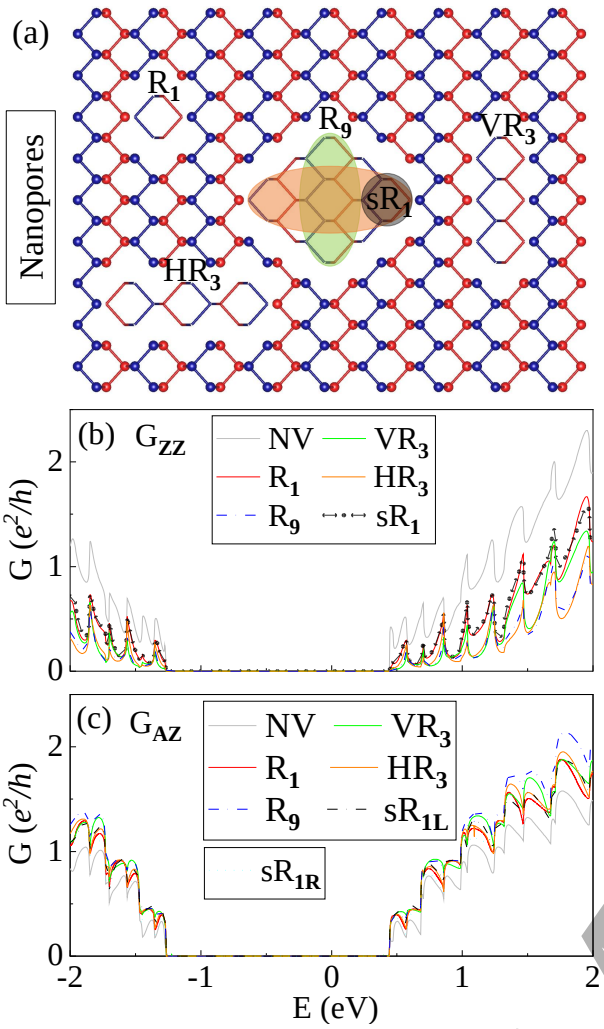

FIG. 9: (a) Schematic diagram of various nanopores labeled by different notations, i.e., R_1, R_9, HR_3, VR_3, and sR_1; (b) [(c)] Longitudinal (transverse) conductance G_{ZZ} (G_{AZ}) of the defective CPNR with R_1, R_9, HR_3, VR_3, and sR_1. In (b) [(c)], the longitudinal (transverse) conductance of the pristine system are shown for comparative purposes.

injection source. This can be explained by the inversion asymmetry between the left and right armchair terminals due to the presence of ADV. These interesting results are supported by the spatial LDOS of the transport modes in the pristine and defective CPNR systems, as shown in Figs. 8(c)-8(f). Here we use solid black triangles to denote the positions of MV, SDV, and ADV in the defective CPNR. The spatial LDOS for each case (NV, MV, SDV, and ADV) were calculated at the energy $E = 1.1$ eV. It is clear from the spatial LDOS that atomic vacancies (MV, SDV, ADV) do render the transport modes be scattered from the longitudinal to transverse direction, and that an asymmetric distribution of the spatial LDOS is observed for the case of ADV.

Now we present and discuss the results obtained by increasing the size of vacancy to include a bunch of atoms, forming the so-called nanopores. We aim to examine the role of such possibly engineered (extrinsic) defects on the conductance of the CPNR system. In Fig. 9(a), five different nanopores are schematically shown and they are named according to missing hexagonal atomic rings (i.e. R_n) and their orientations, where n integer refers to the number of missing rings. Here for instance R_1 (R_9) stands for one (nine) ring of missing atoms at the center of the scattering area. Another two nanopores labeled HR_3 and VR_3 are comprised of R_3 with horizontal and vertical orientations. Following nanopores are also considered at equal distance from each terminal, and their positions are highlighted by horizontal and vertical ellipses at the center of scattering area. Moreover, we also consider by shifting R_1 towards the right terminal of the CPNR system (i.e. sR_1) in order to understand the effect of the nanopore position in the scattering region.

In Figs. 9(b) and 9(c), we show the longitudinal and transverse conductances of the defective CPNR with R_1, R_9, VR_3, HR_3, sR_1 and of the pristine system (NV). As can be seen, the longitudinal conductance (G_ZZ) decreases remarkably by increasing the size of nanopore from R_1 to R_9. Meantime, the transverse conductance (G_AZ) increases due to the decrease of the longitudinal conductance (G_ZZ). The HR_3 nanopore affects the conductance more profoundly than the VR_3 nanopore, which indicates that the orientation of nanopore plays an important role on the electronic transport as well. Moreover, HR_3 and VR_3 result in a more significant decrease (increase) in the longitudinal (transverse) conductance. This is clearly due to the wider interface of the nanopore that is perpendicular (parallel) to the initial transport direction of injection carriers. In addition, the conductance obtained for the sR_1 nanopore exhibits an asymmetry between the two transverse components (denoted by the sR_{1L} and sR_{1R} curves). This conductance asymmetry is induced by the inversion asymmetry of the shifted nanopore in the scattering region.

D. Effect of Vacancy Position

Finally, we present the effect of vacancy position on the transport properties of PNR-based multi-terminal system by considering TPNR-II configuration. In Figs. 10(a) and 10(b), we show the transverse (G_{ZZ}) and longitudinal (G_{AZ}) conductance components of the TPNR-II system for different positions of MV in the scattering region. For illustration purposes, three different positions of MV, as marked by red dots and labeled by C (center) and CL/CR (center to left/right) in the scattering region of the TPNR-II system, are schematically shown in the inset of Fig. 10(a). As can be seen in Figs. 10(a) and 10(b), when MV is located at the right edge (i.e. CR) of the scattering region, it has almost no influence on the conductance components at higher energies, whereas it yields a significant reduction to the in-gap longitudinal conductance (due to in-gap edge modes). This is because

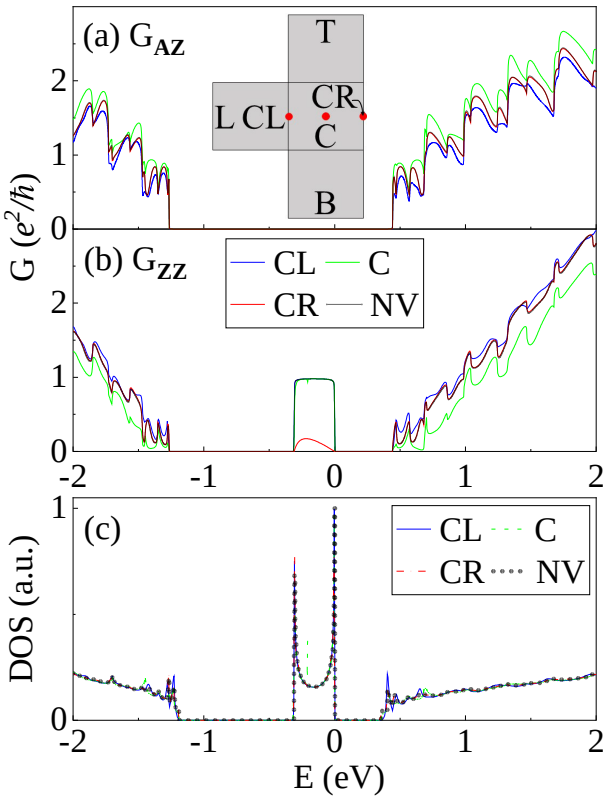

FIG. 10: (a) Transverse conductance, (b) longitudinal conductances, and (c) DOS results for different positions of MV in the TPNR-II system. Here three different positions of MV, as marked by red dots and labeled by C (center) and CL/CR (center to left/right) in the scattering region of the TPNR-II system, are schematically shown in the inset of (a).

the conducting modes in the gap are 1D edge modes that are mainly localized at the zigzag edges of the PNR, while the conducting modes at higher energies are 2D bulk modes that are mainly distributed in the center of the PNR. On the other hand, the transverse (longitudinal) conductance at higher energies is increased (decreased) by shifting the position of MV from CR to C. By further moving MV to the CL position, the transverse (longitudinal) conductivity tends to become decreased (increased). The different behaviors of the transverse and longitudinal conductances induced by changing the MV position are due to the fact that MV plays the role of constructive (destructive) scattering to the transverse (longitudinal) conductance. Moreover, as can be seen in Fig. 10(c), MV located at the C position induces an extra peak in the DOS around the in-gap energies, which however disappears when MV is located at the CL or CR position.

V. CONCLUSIONS

We investigated the electronic transport in pristine and defective PNR-based multi-terminal systems using the NEGF method within the framework of the TB approach. Specifically, we considered three different configurations with two, three, and four terminals which are named as LPNR, TPNR and CPNR, respectively.

We found that for the two-terminal LPNR system the conductance from source to drain is dominated by the armchair terminal, e.g., in-gap conductance of the zigzag terminal is suppressed by the semiconducting nature of armchair terminal. For the three-terminal TPNR system and the four-terminal CPNR system, there are two kinds of conductances of interest, i.e., co-axial (longitudinal) and non-axial (transverse) conductances. In the presence of atomic defects (vacancies and nanopores), the longitudinal (transverse) conductance of these multi-terminal systems exhibits a decrease (an increase) when compared to that of their pristine counterparts. This feature is not present in two-terminal APNR and ZPNR systems where there is only longitudinal conductance that is reduced in the presence of atomic defects. These interesting results can be understood in terms of the spatial LDOS of the transport modes in these multi-terminal systems. Moreover, we found that symmetric and asymmetric nature of atomic defects either vacancies or nanopores result in symmetric and asymmetric distributions of the spatial LDOS these multi-terminal systems. Our results provide fundamental insights into the electronic transport in suspended monolayer PNR-based multi-terminal systems and into the ability of atomic defects to tune the transport properties. When the PNR is placed on a substrate such as SiO_2 or Al_2O_3, the electronic mobility is expected to be reduced by two main scattering mechanisms: (i) the charge impurity (Coulomb potential) scattering from the substrate and (ii) the surface optical phonon scattering between the substrate and the PNR. The mechanism (i) dominates over the electronic scattering at low temperatures whereas the mechanism (ii) plays an important role at high temperatures.

Acknowledgements

This work was supported by the National Key Research and Development Program of China (Grant No. 2016YFA0301700), the NNSFC (Grant No. 11625419), the Strategic Priority Research Program of the CAS (Grant Nos. XDB24030601 and XDB30000000), the Anhui initiative in Quantum information Technologies (Grants No. AHY080000), and the Flemish Science Foundation (FWO-Vl). This work was also supported by the Chinese Academy of Sciences and the World Academy of Science for the advancement of science in developing countries.

[1] K. S. Novoselov, A. K. Geim, S. V. Morozov, D. Jiang, Y. Zhang, S. V. Dubonos, I. V. Grigorieva, and A. A. Firsov, Science **306**, 666 (2004).
[2] B. J. G. V. Radisavljevic Branimir, Radenovic Aleksandra and A. Kis, Nat. Nanotechnol. **6**, 147 (2011).
[3] X. Cai, Y. Luo, B. Liu, and H.-M. Cheng, Chem. Soc. Rev. (2018).
[4] L. Li, Y. Yu, G. J. Ye, Q. Ge, X. Ou, H. Wu, D. Feng, X. H. Chen, and Y. Zhang, Nat. Nanotechnol. **9**, 372 (2014).
[5] P. Chen, N. Li, X. Chen, W.-J. Ong, and X. Zhao, 2D Mater. **5**, 014002 (2017).
[6] Z. Li, C. He, T. Ouyang, C. Zhang, C. Tang, R. A. Römer, and J. Zhong, Phys. Rev. Appl. **9**, 044032 (2018).
[7] C. Chowdhury and A. Datta, J. Phys. Chem. Lett. **8**, 2909 (2017).
[8] H. Liu, A. T. Neal, Z. Zhu, Z. Luo, X. Xu, D. Tománek, and P. D. Ye, ACS Nano **8**, 4033 (2014).
[9] J. Qiao, X. Kong, Z.-X. Hu, F. Yang, and W. Ji, Nat. Commun. **5**, 4475 (2014).
[10] H. O. Churchill and P. Jarillo-Herrero, Nat. Nanotechnol. **9**, 330 (2014).
[11] F. Xia, H. Wang, and Y. Jia, Nat. commun. **5**, 4458 (2014).
[12] A. Carvalho, M. Wang, X. Zhu, A. S. Rodin, H. Su, and A. H. C. Neto, Nat. Rev. Mater. **1**, 16061 (2016).
[13] L. L. Li, B. Partoens, W. Xu, and F. M. Peeters, 2D Mater. **6**, 015032 (2019).
[14] C. Li, Z. Xie, Z. Chen, N. Cheng, J. Wang, and G. Zhu, Materials **11**, 304 (2018).
[15] J. Du, M. Zhang, Z. Guo, J. Chen, X. Zhu, G. Hu, P. Peng, Z. Zheng, and H. Zhang, Sci. Rep. **7**, 42357 (2017).
[16] W. Lu, H. Nan, J. Hong, Y. Chen, C. Zhu, Z. Liang, X. Ma, Z. Ni, C. Jin, and Z. Zhang, Nano Res. **7**, 853 (2014).
[17] V. Tran and L. Yang, Phys. Rev. B **89**, 245407 (2014).
[18] A. Carvalho, A. Rodin, and A. C. Neto, EPL (Europhys. Lett.) **108**, 47005 (2014).
[19] Y. Cai, G. Zhang, and Y.-W. Zhang, Sci. Rep. **4**, 6677 (2014).
[20] F. Liu, Y. Wang, X. Liu, J. Wang, and H. Guo, IEEE Trans. Electron Dev. **61**, 3871 (2014).
[21] R. Zhang, Z. Wu, X. Li, and K. Chang, Phys. Rev. B **95**, 125418 (2017).
[22] J. Yang, S. Tran, J. Wu, S. Che, P. Stepanov, T. Taniguchi, K. Watanabe, H. Baek, D. Smirnov, R. Chen, et al., Nano Lett. **18**, 229 (2017).
[23] S. Das, W. Zhang, M. Demarteau, A. Hoffmann, M. Dubey, and A. Roelofs, Nano Lett. **14**, 5733 (2014).
[24] C. Guo, C. Xia, L. Fang, T. Wang, and Y. Liu, Phys. Chem. Chem. Phys. **18**, 25869 (2016).
[25] X. Han, H. M. Stewart, S. A. Shevlin, C. R. A. Catlow, and Z. X. Guo, Nano Lett. **14**, 4607 (2014).
[26] J. Gao, G. Zhang, and Y.-W. Zhang, Nanoscale **9**, 4219 (2017).
[27] A. Cupo, P. Masih Das, C.-C. Chien, G. Danda, N. Kharche, D. Tristant, M. DrndicÌĄ, and V. Meunier, ACS Nano **11**, 7494 (2017).
[28] B. Kiraly, N. Hauptmann, A. N. Rudenko, M. I. Katsnelson, and A. A. Khajetoorians, Nano Lett. **17**, 3607 (2017).
[29] L. L. Li and F. M. Peeters, Phys. Rev. B **97**, 075414 (2018).
[30] S. C. Dhanabalan, J. S. Ponraj, Z. Guo, S. Li, Q. Bao, and H. Zhang, Adv. Sci. **4**, 1600305 (2017).
[31] W. Hu and J. Yang, J. Phys. Chem. C **119**, 20474 (2015).
[32] T. Jayasekera and J. Mintmire, Nanotechnology **18**, 424033 (2007).
[33] G. Thorgilsson, G. Viktorsson, and S. Erlingsson, J. Comput. Phys. **261**, 256 (2014).
[34] L. R. Lima, A. Dusko, and C. Lewenkopf, Phys. Rev. B **97**, 165405 (2018).
[35] A. N. Rudenko and M. I. Katsnelson, Phys. Rev. B **89**, 201408 (2014).
[36] S. Datta, *Electronic transport in mesoscopic systems* (Cambridge university press, 1997).
[37] M. L. Sancho, J. L. Sancho, J. L. Sancho, and J. Rubio, J. Phys. F: Met. Phys. **15**, 851 (1985).
[38] L. Huang, Y.-C. Lai, D. K. Ferry, R. Akis, and S. M. Goodnick, J. Phys.: Condens. Matter **21**, 344203 (2009).
[39] M. Ezawa, New J. Phys. **16**, 115004 (2014).